# Numerical Computation of Inception Point Location for Steeply Sloping Stepped Spillways

**Mohammad Sarfaraz[1], Jalal Attari[2] and Michael Pfister[3]**

**1- Graduate Student, Department of Civil Engineering, Sharif University of Technology, Iran**
**2- Assistant Professor, Power and Water University of Technology, Iran**
**3- Ph.D., Laboratory of Hydraulic Constructions (LCH), Ecole Polytechnique Fédérale de Lausanne (EPFL), Lausanne, Switzerland**

mohammad.sarfaraz@gmail.com

**Abstract**

Stepped spillways have gained much interest in recent decades because of their compatibility with Roller Compacted Concrete (RCC) dams. Hydraulics of stepped spillways is not simple considering different flow regimes and regions along the chute. Estimation of flow characteristics of the stepped chutes is presently carried out by using some empirical formulae and physical modeling, which are partially inaccurate if scaled up due to scale effects produced by high interaction between air and water. However, this can be improved by application of Computational Fluid Dynamics (CFD) models. The inception point of aeration of stepped spillways is placed further upstream than on smooth spillways. The position of this point is relevant to cavitation potential, flow losses and flow depth; hence an accurate approximation of the inception point location is essential. In this paper, flow characteristics with emphasis of investigating air concentration in a stepped spillway having a steep slope, was computed by a commercial CFD program. A comparison of the numerical and physical model results showed a relatively good agreement. The study indicates that the turbulence numerical simulation is an effective and useful method for the complex stepped spillway overflow.

**Keywords: Stepped Spillway, Air Entrainment, Inception Point, Numerical Modeling, Large Eddy Simulation**

## 1. INTRODUCTION

Stepped spillways are found to be effective for energy dissipation of excess flood released from dams. Many studies have shown that favorable design of stepped spillways can decrease the size of the stilling basin significantly and thus saving on construction costs [1, 2]. Stepped spillways have gained much interest in recent decades because of their compatibility with Roller Compacted Concrete (RCC) dams, hence having a steep slope of more than 50°. Once a stepped chute is located on the body of a RCC dam, it offers additional constructional and economic advantages [3].

On stepped chutes with skimming flow regime, the flow is highly turbulent. Once the outer edge of the turbulent boundary layer reaches the free surface, natural air entrainment commences [2]. $L_i$ designates the distance, along the chute, between the ogee crest and the section where the air entrains the free surface. The thickness of the aerated zone then increases, protruding to the steps, so that the entire flow turns out to be aerated [4]. $L_{ib}$ assigns the distance, along the chute, between the ogee crest and the section of developing fully aerated flow (Figure 1). Sufficient air entrainment about 5% at the spillway surface eliminates cavitation risk and will affect training wall design [3, 4]. Hence a proper estimate of this parameter is essential in the first design of stepped spillways, to assure that air entrainment will appear on the chute and its magnitude is high enough to prevent cavitation damages.

Engineers and researchers are often challenged with stepped spillways. There are only few empirical formulae for estimating inception point location ($L_i$), which can be used for wide range of stepped spillways [e.g. 5, 6]. Also because of complex existing hydraulic of air-water flow in stepped spillways, no explicit criterion has been presented to design in term of air concentration distribution to prevent cavitation risk [3, 5,].

Physical modeling is limited in investigating flow characteristics in all spatial details, because intrusive measurements in the step niches will disturb the vortex generated there. On the other hand, due to highly aerated flow in stepped spillways, scaling up their physical modeling results will result in scale effects if not adequately performed [2, 3]. Nowadays, with availability of high performance computers and CFD codes, flow characteristics over hydraulic structures can be accurately estimated, which are highly needed for design purposes. The aim of this research is to (1) assure that numerical modeling can be reliable as physical

model testing to study air-water flow characteristics by means of its verification with an experimental study, (2) numerically calculate the inception point location ($L_i$ and $L_{ib}$) and (3) numerically estimate air concentration distribution at different locations along the stepped chute.

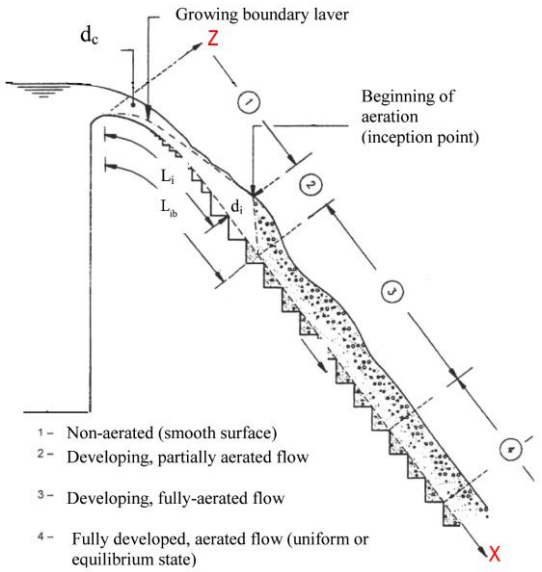


**Figure 1. Flow regions in the skimming flow regime (after [5])**

## 2. PHYSICAL MODEL

The experimental work performed by Pfister and Hager [7] was used to verify the numerical modeling results. The channel was 0.5 m wide and 3.4 m long. An ogee profile at its upstream end, joined to a stepped chute with the angle (α) of 50° containing 25 steps with height (h) of 0.093m was used (Figure 2). Coordinate defined in Figures 1 (X, Z) and Figure 2 (X', Z') are different from each other.

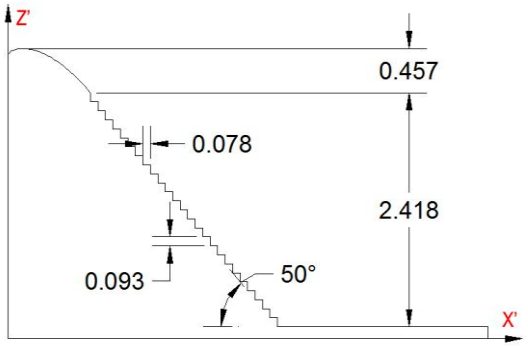


**Figure 2. Configuration of experimental work, dimensions in meters. [7]**

The test program included six discharges (table 1). The air concentration (C) distribution was measured with a fiber-optical probe. The profiles were measured at step edges perpendicular to the pseudo-bottom to the flow surface ($d_{90}$). No measurements were taken within the step niches. It is important to note that no air entrainment occurs in the last test as the test reach was too short, which could lead into cavitation risks for prototype conditions and this phenomena must be taken into accounts in the design procedure.

**Table 1- Test program, introductory values**

| Test no. | q ($m^3$/s.m) | $d_c$/h | $L_{ib}$(m) |
|---|---|---|---|
| 1 | 0.108 | 1.1 | 1.09 |
| 2 | 0.215 | 1.8 | 1.53 |
| 3 | 0.322 | 2.4 | 2.17 |
| 4 | 0.430 | 2.9 | 2.55 |
| 5 | 0.537 | 3.3 | 3.18 |
| 6 | 0.646 | 3.8 | – |

## 3. NUMERICAL IMPLEMENTATION

The commercially available Computational Fluid Dynamics program, Flow-3D was used for solving the Reynolds-averaged Navier-Stokes equations in combination with two eddy-viscosity closure models to take account of turbulence. The solver uses finite volume approximation to discretize the computational domain. The pressure and velocity are coupled implicitly by using the time-advanced pressures in the momentum equations and time-advanced velocities in the continuity equations. Turbulence was encountered by both RNG k-ε and Large Eddy Simulation (LES).

### 3.1. Governing Equations

The continuity and momentum equations for fluid flow and transport equation for VOF function are [8]:

$$\frac{V_f}{\rho}\frac{\partial \rho}{\partial t}+\frac{1}{\rho}\nabla.\left(\rho \vec{u}A_f\right)=-\frac{\partial V_f}{\partial t} \tag{1}$$

$$\frac{\partial \vec{u}}{\partial t}+\frac{1}{V_f}\left(\vec{u}A_f.\nabla \vec{u}\right)=-\frac{1}{\rho}\left[\nabla P+\nabla.\left(\tau A_f\right)\right]+\vec{G} \tag{2}$$

$$\frac{\partial F}{\partial t}+\frac{1}{V_f}\nabla.\left(F\vec{u}A_f\right)=-\frac{F}{V_f}\frac{\partial V_f}{\partial t} \tag{3}$$

Where ρ is fluid density, $\vec{u}$ fluid velocity, $V_f$ volume fraction, $A_f$ area fraction, P pressure, τ viscous stress tensor, G gravity and F is fluid fraction.

The RANS model includes two transport equations for the turbulent kinetic energy (k) and the rate of turbulence dissipation (ε) to obtain the Reynolds stress $\left(\overline{u_i u_j}\right)$ and the turbulent viscosity ($\upsilon_t$) [8]:

$$-\overline{u_i u_j}=\upsilon_t\left(\frac{\partial u_i}{\partial x_j}+\frac{\partial u_j}{\partial x_i}\right)-\frac{2}{3}\delta_{ij}k \tag{4-a}$$

$$\upsilon_t=c_\mu\frac{k^2}{\varepsilon} \tag{4-b}$$

The physics of air entrainment to the turbulent flow is shown in Figure 4. When the turbulence in the flow is sufficiently high to disturb the stabilization of water surface, air entrainment occurs when:

Turbulent energy uplift ($P_t$) > Surface stabilizing forces of gravity and surface tension ($P_d$) [9] (5-a)

$$\rho k > \underbrace{\rho g_n L_t}_{\text{Body force}} + \underbrace{\frac{\sigma}{L_t}}_{\text{Surface tension force}} \tag{5-b}$$

where k = turbulent kinetic energy, ρ = liquid density, σ = the coefficient of water surface tension, $g_n$ = the component of gravity normal to the free surface and $L_t$ = raised height for the fluid element.

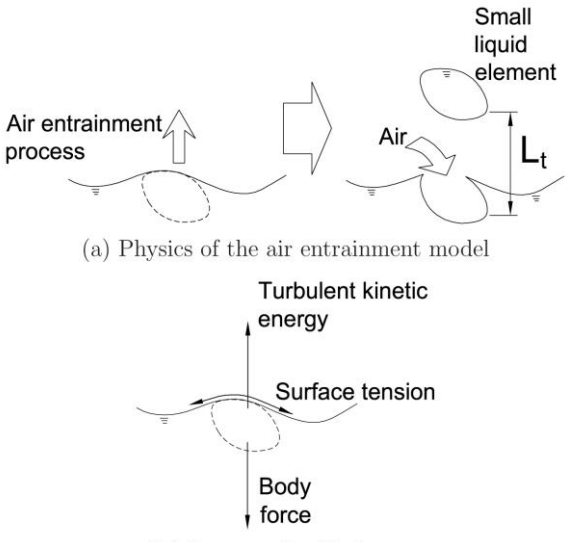


**Figure 4. Air entrainment mechanism (after [3])**

For the smooth solid boundary, it is assumed that the center of the element closest to a solid boundary is within the log layer of the wall; hence the logarithmic velocity distribution is adopted:

$$\frac{u}{u_*} = \frac{1}{\kappa}\ln\frac{u_* z}{\upsilon} + 5.0 \tag{6}$$

Where $u_*$= shear velocity; $\kappa$=von Kármán constant equal to 0.41, and z=distance from the boundary.
For the LES, the Gaussian function (7) was chosen as the kernel of the filter. Also Smagorinsky-Lilly sub-grid scale model (8) was selected to simulate the minor eddies in this study.

$$G\left(x-\xi\right) = \left(\frac{\varsigma}{\pi\Delta^2}\right)^{0.5} \exp\left(\frac{-\varsigma\left(x-\xi\right)^2}{\Delta^2}\right) \tag{7}$$

$$\upsilon_t = \left(C_s\Delta\right)^2\sqrt{2S_{ij}S_{ij}} \tag{8}$$

Where $\Delta$= eddy size cut-off depending on the mesh size, $C_s$=0.18, $\varsigma$ = 6 and $S_{ij}$ is denoted by (9), in which $\tilde{u}_i$ is the spatially filtered velocity:

$$S_{ij} = \frac{1}{2}\left(\frac{\partial\tilde{u}_i}{\partial x_j} + \frac{\partial\tilde{u}_j}{\partial x_i}\right) \tag{9}$$

3.2. Model Setup
The numerical model was carried out in 2D domain. 750000 uniform sized meshes were used to discretize the domain. Boundary conditions for $z_{max}$ and y directions were symmetry, i.e. free slip condition. $x_{min}$ was selected as the stagnation pressure, simulating the flow entering to the domain with zero velocity from a reservoir. For the $x_{max}$ the outflow condition was employed to allow the fluid leave the domain.

## 4. NUMERICAL RESULTS AND ANALYSIS

The numerical methodology was applied to the experimental work by Pfister and Hager [7] and results of both numerical and experimental data is compared and discussed. Table 2 presents experimental and numerical values of $L_{ib}$ and $L_i$ computed by the two turbulence models. The parameter $L_i$ was not measured in the physical model and the relative errors are computed for $L_{ib}$. It points out that LES turbulence model is more accurate than RNG k-ε to calculate $L_{ib}$., therefore it was chosen for presenting other simulated results.

**Table 2- Comparison of experimental and computed values of $L_{ib}$ and $L_i$**

| q ($m^3$/s.m) | Experimental | Numerical | | | | | |
|---|---|---|---|---|---|---|---|
| | $L_{ib}$(m) | Renormalized Group k-ε | | | Large Eddy Simulation | | |
| | | $L_i$(m) | $L_{ib}$(m) | Relative Error (%) | $L_i$(m) | $L_{ib}$(m) | Relative Error (%) |
| 0.108 | 1.09 | 1.0826 | 1.2372 | 13.5046 | 0.9795 | 1.1351 | 4.1376 |
| 0.215 | 1.53 | 1.4564 | 1.6318 | 6.6536 | 1.3994 | 1.5861 | 3.6667 |
| 0.322 | 2.17 | 1.5798 | 1.9746 | 9.0046 | 1.6016 | 2.0837 | 3.9770 |
| 0.430 | 2.55 | 2.2375 | 2.804 | 9.9608 | 1.8349 | 2.5036 | 1.8196 |
| 0.537 | 3.18 | 2.8268 | 2.8303 | 10.9969 | 2.7525 | 3.2346 | 1.7170 |
| 0.646 | – | 3.3246 | – | – | 3.1724 | – | – |

Figure 5. shows comparison of measured $L_{ib}$ and LES computed $L_{ib}$ and $L_i$ normalized with $k_s$ equal to h.cosα. The parameter $F_*$ is the roughness Froude number, which is calculated through equation (10):

$$F_* = \frac{q}{\sqrt{g\sin\alpha k_s^3}} \tag{10}$$

This figure shows that the numerical model is well capable enough to compute $L_{ib}$. Also it is revealed that at low discharges, $L_i$ is close to the $L_{ib}$, but as discharge increases the difference between these two values gets larger; hence $L_i$ is not a suitable parameter for investigation of cavitation potential along the chute. It is remarkable that for q=0.646 $m^3$/sm, air does not reach the bottom of the step along the chute, while air entrainment initiate from the surface ($L_i$).

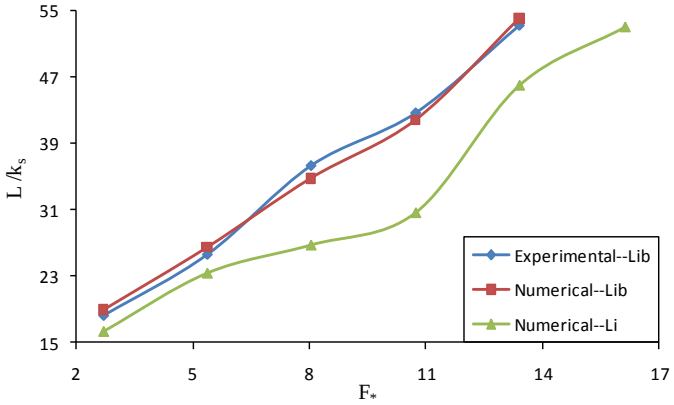


**Figure 5. Comparison of measured $L_{ib}$ and numerically-derived $L_{ib}$ and $L_i$ for different discharges ($F_*$)**

Numerically-derived distributions of volume fraction of water (1-C) for all discharges are demonstrated in Figure 6. This figure illustrates that by increasing discharge, the location of inception point moves toward the downstream, which for the last discharge, no air entrainment occurs along the chute.

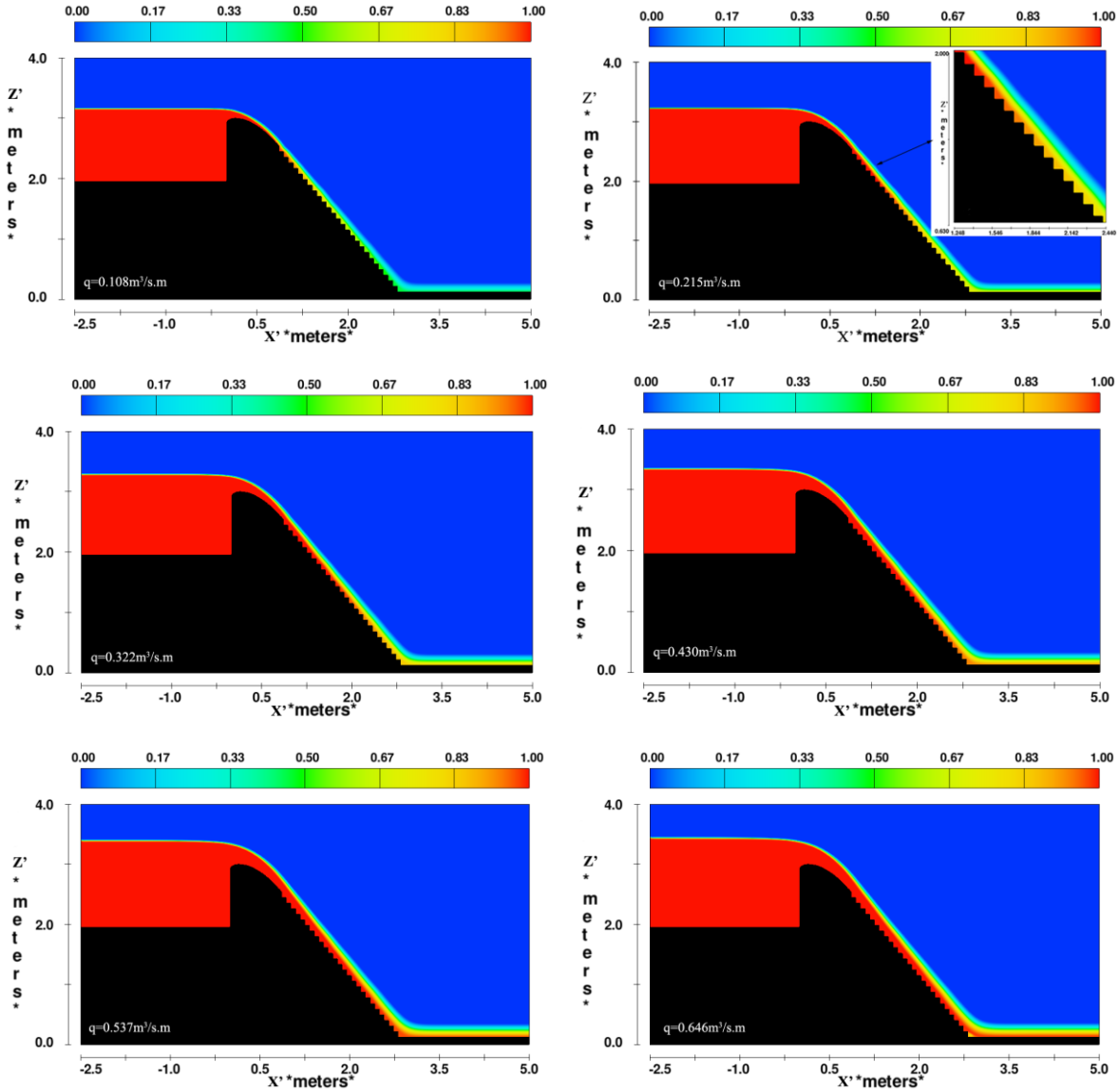


**Figure 6. Numerical computation of two phase flow along the stepped chute for different discharges**

In Figure 7, experimental and computed air concentration distribution at different locations for discharge of 0.215 ($m^3$/sm) is presented. This figure indicates that numerical method is well accurate and reliable enough to estimate air concentration. It is also shown that LES turbulence model is more accurate than RNG k-ε.

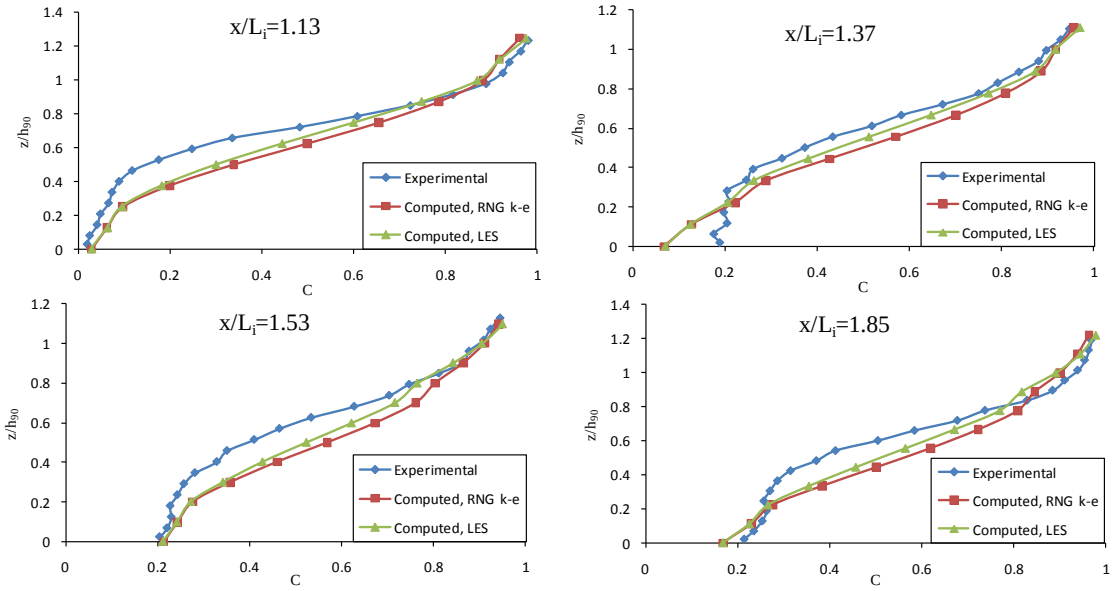


**Figure 7. Measured and numerically-derived Air concentration distribution at different positions, q=0.215**

In Figure 8. experimental and computational air concentration distribution for q=0.537 $m^3$/s.m is presented. In this discharge, the locations of measurements lie in the region of $x/L_{ib} \leq 1$, where the turbulence in the flow is not sufficiently high to disturb the stabilization of water surface to make the air reach the bottom. It is obvious that numerical model is capable of computing air concentration in such regions.

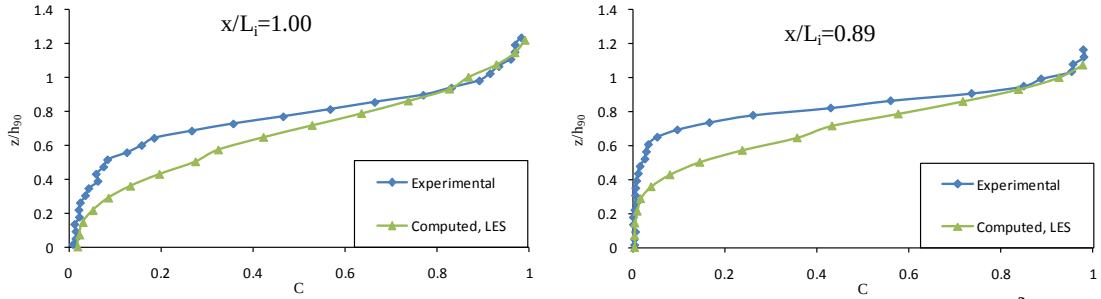


**Figure 8. Measured and numerically-derived Air concentration distribution at two positions, q=0.537 $m^3$/s.m**

In Figure 9 numerically-derived air concentration distribution along the vertical axis (z') perpendicular to the middle of the 6th step bottom (x'=1.28 m) is presented. It is clear that by increasing discharge, bottom and mean air concentration decreases, which for discharges larger than 0.322 $m^3$/s.m no air reaches the bottom. Also the local rate of air entrainment (slope of the diagram) decreases by increasing the discharge. It should be noted that no measurements were performed by [7] in the inner part of the step, due to disturbing generated vortex in that region by inserting the probe. Others however were measuring these concentrations [10].

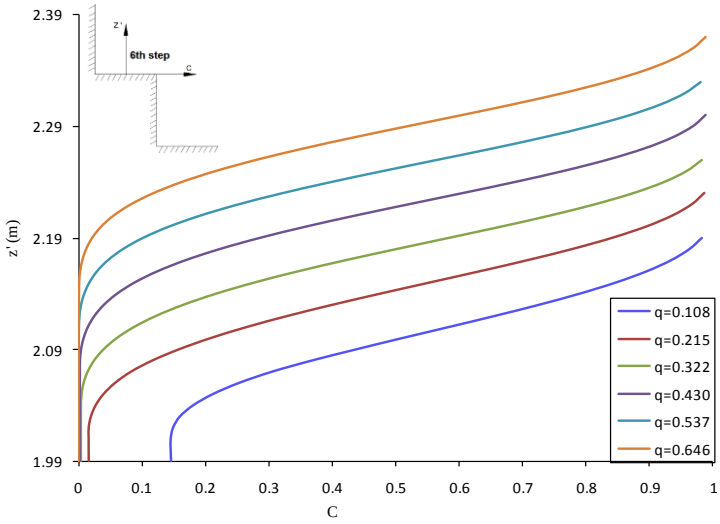


**Figure 9. Numerically-computed air concentration distribution perpendicular to the middle of 6th step bottom for different discharges ($m^3$/s.m)**

Figure 10. demonstrates velocity vectors together with pressure in a step niche within the numerical modeling results. The figure indicates that the minimum value of pressure exist in the outer edge of the step, close to the vertical wall, which is reported by several other investigators [e.g. 2]. This is caused by flow separation in this region when it leaves the step which is clearly shown in the picture by the velocity vectors going out the step edge. Also maximum pressure is located in the horizontal wall of the step near the edge, caused by impact of flow coming from the upper step.

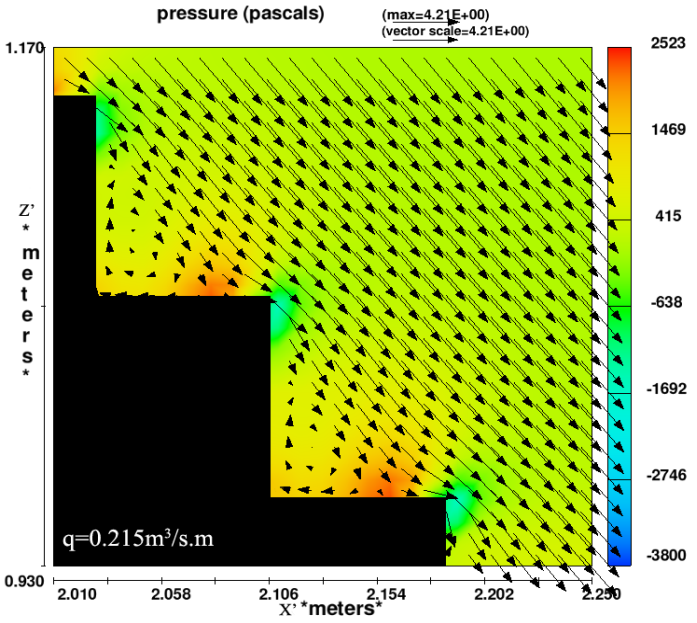


**Figure 10. Velocity vector together with pressure distribution, q=0.215 $m^3$/s.m.**

## 5. CONCLUSIONS

In this paper, a numerical analysis was performed to simulate and investigate flow characteristics over a steeply sloping stepped spillway. The computational results were compared with the experimental data in two respects: location of inception of aeration and air concentration distribution. On the basis of results, the following conclusions can be drawn:

- LES was recognized an accurate turbulence model with the VOF method to study the stepped spillway air water interaction successfully. The numerical procedure proposed in this paper is well capable to predict air concentration distribution, which is necessary for investigating cavitation potential risk in stepped spillways.
- By increasing the discharge, location of the inception shifts towards downstream of the stepped chute. Also bottom, mean air concentration and rate of air entrainment decrease locally, which supports cavitation potential risks at high discharges.
- As the discharge increase, the distance between $L_i$ and $L_{ib}$ raises, i.e. it takes more distance for air to reach the bottom from surface of water. This indicates that $L_i$ is not a proper parameter to study the cavitation potential risk.
- Minimum and maximum values of pressure exist in the outer edge and the horizontal part of the step near the edge of the step respectively.
- Considering advantages of the CFD models (e.g. less time and lower cost), flow simulation can be performed by application of numerical models. These models should be joined with the physical model studies to perform better design and understand the flow behavior more accurately.

## 6. ACKNOWLEDGMENT

Flow Science Incorporation is gratefully acknowledged for allowing the authors to use their excellent software, Flow-3D. Also the first author is grateful to Dr. Michael Barkhudarov, the vice president of research & development of Flow Science Inc., for his suggestions and helps.

## 7. REFERENCES

1. Chanson, H. (2001). *"The Hydraulics of Stepped Chutes and Spillways"*, A. A.Balkema, Lisse, pp. 375.

2. Minor, H.E., and Hager, W.H. (2000). *"Hydraulics of Stepped Spillways"*, A. A.Balkema, Rotterdam, pp. 201.

3. Sarfaraz, M. (2010). *"Hydraulic Design and Modeling of Stepped Spillways Located on RCC Dams, Case Study: Javeh RCC Dam"*, BSc. thesis, Power and Water University of Technology, Tehran, Iran.

4. Boes, R.M., Hager, W.H., (2003), *"Two-Phase Flow Characteristics of Stepped Spillways"*, Journal of Hydraulic Engineering 129(9), 661-670.

5. Sarfaraz, M., Pfister, M., Attari, J. and Sarfaraz, H. (2012). *"Systematic Comparison of Design Proposals for Stepped Spillways with Representative Model Data"*, 1st International Conference on Dam and Hydropower Engineering, Tehran, Iran.

6. Sarfaraz, M. and Attari, J. (2011), *"Selection of Empirical Formulae for Design of Stepped Spillways on RCC Dams"*, Proceeding of the World Environmental and Water Resources Congress (EWRI), Palm Spring, California, U.S.A.

7. Pfister, M. and Hager, W.H., (2010), "*Self-Entrainment of Air on Stepped Spillways"*, International Journal of Multiphase Flow 37(2), 99-107

8. Flow Science, Incorporated, (2008), *"FLOW-3D Users Manual Version 9.3"*, Santa Fe, New Mexico.

9. Sarfaraz, M., Attari, J. and Maroofi, N. (2011). *"Numerical Calculation of Inception Point Location for Mildly Sloping Stepped Spillways"*, 10th Iran's Hydraulic Conference, Guilan University, Rasht, Iran, (in Farsi).

10. Boes, R.M., (2000), *"Zweiphasenströmung und Energieumsetzung an Grosskaskaden"*, VAW *Mitteilungen* no. 166, H.-E. Minor, ed. ETH: Zurich, (in German).